Diagn Interv Radiol 2019; 25:257–264

ABDOMINAL IMAGING

ORIGINAL ARTICLE

Low tube voltage increases the diagnostic performance of dual-energy computed tomography in patients with acute appendicitis

Çağdaş Topel
Mehmet Ruhi Onur
Erhan Akpınar
Ali Devrim Karaosmanoğlu
Deniz Akata
Muşturay Karçaaltıncaba

PURPOSE
We aimed to assess the utility of dual-energy computed tomography (DECT) imaging in diagnosing acute appendicitis (AA) with density measurements of the appendix vermiformis.

METHODS
A total of 210 consecutive patients presenting with acute abdominal pain were scanned using DECT between January and October 2016. Twenty-six patients had pathologically confirmed AA, while 30 had normal appendices. Appendiceal densities were measured in the true axial section of the appendix vermiformis at 80 kVp, 140 kVp, virtual noncontrast, iodine overlay, mixed, and monoenergetic (40, 50, 60, 70, 80, 90, 100 keV) images.

RESULTS
Comparison of the appendix at different kVp and keV energy levels, virtual noncontrast, iodine overlay, and mixed images yielded significant differences between patients with appendicitis and those with a normal appendix ($P < 0.001$ for all). Receiver operating characteristic (ROC) curve analysis revealed that the 80 kVp image set yielded the best diagnostic performance among all image sets (area under the ROC curve [AUC], 0.996; $P < 0.001$), while 70 keV images yielded the highest diagnostic performance among the virtual monoenergetic image sets (AUC, 0.958; $P < 0.001$). Inter-rater agreement was good at 80 kVp images (intraclass correlation coefficient [ICC], 0.78, $P < 0.001$).

CONCLUSION
Evaluation of DECT image reconstructions suggested that low tube voltage with 80 kVp demonstrated accurate diagnostic performance for AA. This finding suggests that low kVp CT may be useful for diagnosing AA with reduced patient radiation exposure.

Acute appendicitis (AA) remains the most common indication for emergency surgery. False-positive rates of 10%–20% among individuals who undergo surgery for AA were within acceptable limits in the past, with higher rates of up to 40% in women of child-bearing age before the era of computed tomography (CT) (1).

Numerous studies have been performed to assess the diagnostic performance of CT in diagnosing AA. In a systematic review describing the high utility of CT as a diagnostic tool for AA, sensitivity and specificity rates of 94% and 95%, respectively, were reported (2). Despite its notable diagnostic performance for patients with suspected appendicitis, the proper CT protocol and acceptable patient radiation exposure limits remain controversial issues and are also the subject of ongoing research (3–6). In addition, contrast enhancement of the appendix vermiformis has not been evaluated yet.

Dual-energy CT (DECT) is a diagnostic tool that capitalizes on the varying attenuation of tissues at different X-ray energy levels. This technique facilitates the detection of iodine-containing tissues at low energy levels and also enables the reconstruction of virtual noncontrast (VNC) images. DECT primarily relies on obtaining two datasets from the same anatomical location at different X-ray energies (usually 80 kVp and 140 kVp) (7). In angiographic scans of the thorax and abdomen using low keV energy levels, it has been reported that increased attenuation values may enable the detection of more subtle contrast enhancement compared with conventional polychromatic imaging (8, 9).

This research was orally presented at ESGAR 2017 in Athens under the title "Evaluation of acute appendicitis with dual-energy CT".

From the Clinic of Radiology (Ç.T. ✉ *cgdstpl@gmail.com*), Ağrı State Hospital, Ağrı, Turkey; Department of Radiology (M.R.O., E.A., A.D.K., D.A., M.K.), Hacettepe University School of Medicine, Ankara, Turkey.

Received 18 December 2018; revision requested 07 January 2019; last revision received 03 March 2019; accepted 16 April 2019.

Published online 18 June 2019.

DOI 10.5152/dir.2019.18567

You may cite this article as: Topel Ç, Onur MR, Akpınar E, Karaosmanoğlu AD, Akata D, Karcaaltıncaba M. Low tube voltage increases the diagnostic performance of dual-energy computed tomography in patients with acute appendicitis. Diagn Interv Radiol 2019; 25:257–264.

There has been a gradual increase in the use of DECT in the field of abdominal radiology. In the present study, we aimed to evaluate DECT imaging in the diagnosis of AA to quantitatively compare the diagnostic performance of different image sets in the detection of appendiceal mural enhancement; quantitatively assess the density values of the appendix vermiformis in Hounsfield units (HU) in patients with and without AA using the scale of virtual monoenergetic imaging (VMI) levels to determine the ideal keV for assessing appendiceal mural enhancement; and, finally, assess the diagnostic value of VNC images in the diagnosis of AA.

Methods

Study population

Ethics approval for this prospective study was obtained from the institutional ethics review board (protocol number: 16969557-576, decision number: GO 16/250–08). After written informed consent was obtained for both CT scanning and study participation, 210 consecutive patients with acute abdominal pain and indeterminate ultrasound results underwent abdominal CT examination between January and October 2016 using a standardized protocol and a DECT system. Individuals <18 years of age and those who were pregnant or unable to receive iodinated intravenous (IV) contrast agent due to renal failure and/or history of contrast agent reaction were excluded. The CT criteria for the diagnosis of AA included a dilated appendix with distended lumen (> 6 mm), and at least one of following findings: wall thickening and enhancement; periappendiceal inflammation, including adjacent fat stranding and thickening of the lateroconal fascia or mesoappendix; extraluminal fluid or abscess formation; or the presence of appendicoliths (10–15).

Main points

- DECT facilitated the detection of iodine-containing tissues at low energy levels and also enabled the reconstruction of virtual noncontrast images.
- Analyses of DECT image sets revealed that the 80 kVp image set yielded excellent diagnostic performance for AA.
- The energy level with the highest diagnostic performance among the monoenergetic image sets was 70 keV.

Reference standard

Because surgical removal of an inflamed appendix is the preferred first-choice treatment for adults in our local institution, the gross pathologic and histopathologic description of surgical specimens based on the final pathology reports (which served as the reference standard for the diagnosis of AA) were reviewed. The histopathologic descriptions in the final pathology reports which were considered to be indicative of AA were as follows: mucosal ulceration, mild to intense infiltration of neutrophils in the muscularis propria with associated necrosis, and congestion and perivascular neutrophilic infiltration (16). The gross descriptions were considered to indicate AA if they contained ≥1 of the following terms: fibrinopurulent exudate on serosa, prominent vessels, lumen contains blood-tinged pus, variable perforation, mucosal ulceration, appendicoliths, or another obstructing agent (16). Patients were diagnosed with AA if the final pathology report included at least one term from both histopathologic and gross descriptions that revealed inflammation of the appendix vermiformis wall.

Control group

To control the measurement of normal appendix, individuals without any of the following conditions that may have had an indirect effect on appendiceal HU value were included: pelvic inflammatory disease, inflammatory bowel disease, significant pelvic fluid or ascites, and any inflammatory changes due to other causes in the right lower quadrant. Adequate intra-abdominal fat tissue was also sought, which enabled thorough measurement. Patients in the control group underwent DECT examination using the same protocol applied to those with pathologically proven AA.

CT acquisition

All CT images were acquired using a dual-source, multi-row detector CT system (Siemens SOMATOM definition, Dual source). One liter of water was used as a negative oral contrast agent in compliant patients, which was consumed in 1 h to 1.5 h, and 30 min before CT. Iodinated oral contrast agent was not administered because it could alter density measurements due to its luminal presence or artifacts. No rectal contrast agent was administered. After acquiring anteroposterior and mediolateral scout views, 1.5 mL/kg of IV contrast agent was administered (Omnipaque [300 mg I/mL], GE Healthcare) at a rate of 3 mL/s followed by 20 mL of 0.9% NaCl at the same injection rate. The datasets were acquired in the portal venous phase (70 s post-injection) using a dual-source (tube A and B), dual-energy (140 kVp and 80 kVp) X-ray tube, with a 0.9 pitch helical acquisition and tube rotation time of 0.5 s. Quality reference levels for current in tubes A and B were 90 mAs and 382 mAs, respectively. Automatic tube current modulation (CARE dose 4D) was used for radiation dose reduction. Abdominal regions of interest (ROI) in all patients were confined to the field of view of the DECT device.

CT image reconstruction

CT images were acquired using 14×1.2 mm collimation and subsequently reconstructed to 5 mm and 1.5 mm slice thickness with an increment value of 1.5 mm. Axial source data from the 140 kVp and 80 kVp scans were reconstructed using the kernel of D30f medium smooth abdomen. The iterative reconstruction technique was not used. Reconstructed images were transferred through the institutional picture archiving communication system (PACS) to the multimodality workstation (Syngo MMWP VE 36A, Siemens Healthcare). Using the liver VNC application, VNC images were reconstructed. As for the dual-energy monoenergetic application, scans were reconstructed at VMI energy levels from 40 to 100 keV in 10 keV increments. The mixed image datasets served as the conventional polychromatic images, which were the reconstruction of fused 80 kVp and 140 kVp datasets.

Quantitative image analysis

For quantitative image analysis, a true axial reformatted image of the appendix vermiformis was obtained by adjusting the reference lines on sagittal and coronal images (Fig. 1a). The most compressed site of the appendix, which was devoid of any appendicoliths, was then explored. In most cases, the most compressed site was found to be on the proximal half of the appendix, immediately before the beginning of the distention. ROIs were placed in consensus at the wall of appendix vermiformis on true axial images by a radiology resident with 5 years of experience in radiology and a staff radiologist with 12 years of experience in abdominal imaging. Three circular ROIs of 0.5 cm^2 were placed on each appendix wall, and the mean attenuation value in HU was recorded. Attention was devoted to mini-

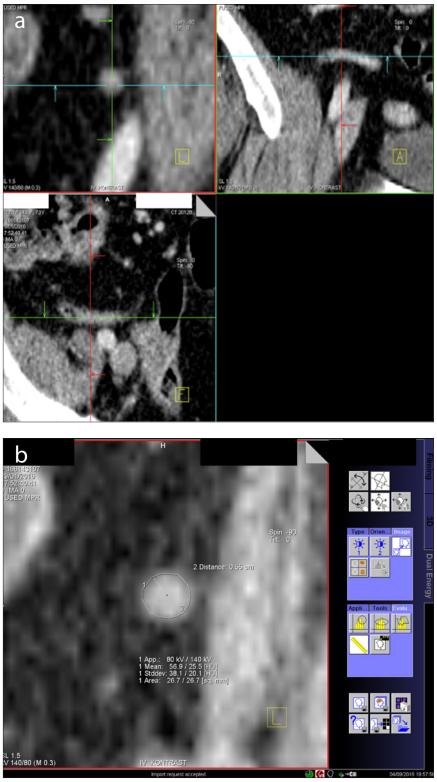

Figure 1. a, b. An example of appendiceal density measurement. Panel **(a)** shows the acquisition of true axial image (left upper image) through coronal and sagittal computed tomography (CT) images. Panel **(b)** shows the measurement of appendiceal density in the reformatted true axial image of appendix vermiformis.

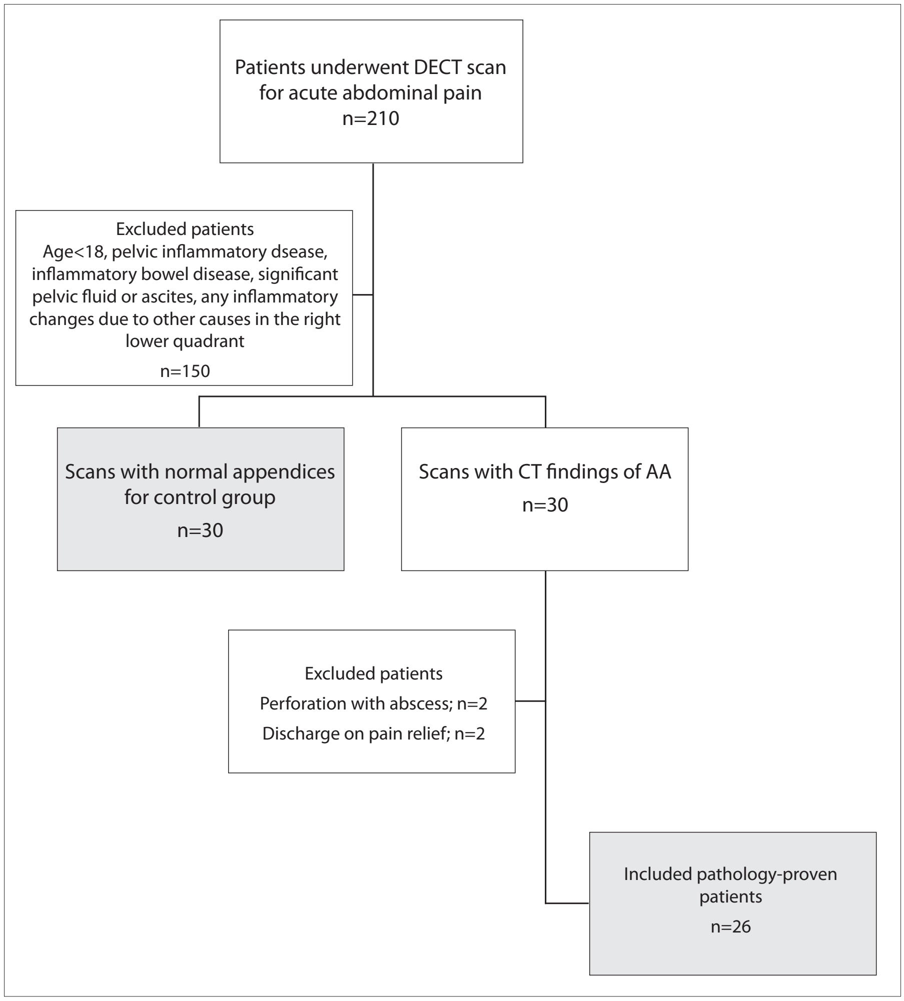

Figure 2. Flow chart illustrating patient distribution.

mize any contamination from appendiceal luminal content and other adjacent peri-appendiceal anatomical structures (Fig. 1b). The maximum diameter of the appendix vermiformis, the density of the most compressed site of the appendix vermiformis at 80 kVp and 140 kVp, VNC, iodine overlay, mixed, and monoenergetic (40, 50, 60, 70, 80, 90, 100 keV) images were recorded.

Statistical analysis

Statistical analyses were performed using SPSS version 23.0 (IBM Corp.) for Windows (Microsoft Corp.). The variables were investigated using visual (histograms and probability plots) and analytical methods (Shapiro-Wilk's test) to determine whether they were normally distributed. Descriptive analyses are presented as mean and standard deviation (SD) for normally distributed variables, and median and interquartile range (IQR) for non-normally distributed variables. The Student's t-test and Mann-Whitney U test were used to compare variables; $P < 0.05$ was considered as statistically significant. The capacity of appendiceal densities in the different image datasets in predicting the presence of AA were analyzed using receiver operating characteristic (ROC) curve analysis. When a significant cutoff value was observed, the sensitivity, specificity, and positive predictive value (PPV) and negative predictive value (NPV) were calculated using MedCalc version 18.6 (MedCalc Software). While evaluating the area under the ROC curve (AUC), a 5% type-1 error was used to accept a statistically significant predictive value of the test variables. To assess inter-rater agreement, 10 patients were randomly selected from each of the groups at 80 kVp images and intraclass correlation coefficient (ICC) was calculated based on two way mixed model, absolute agreement with a mean-rating (k=2). A 95% confidence interval (CI) was applied for all analyses.

Results

Thirty patients with CT-confirmed AA were enrolled in the present study, and appendectomy was performed in 26 patients (86.7%). Two patients (6.6%) who were diagnosed with a perforated appendix and abscess formation were treated using abscess drainage in the interventional radiology unit, and 2 (6.6%) were discharged after IV antibiotic treatment and pain relief. Therefore, four patients whose CT findings met the criteria for AA, but were not operated, were excluded from the study due to the lack of final confirmatory pathology reports. Thirty patients were enrolled as controls for measuring normal appendix HU values. Patient composition in the present study is given in detail in Fig. 2.

In the AA group, 46% of the patients were male (n=12) and 54% were female (n=14), with an age range of 18 to 66 years. The mean age was 36.3±14.1 years. Forty percent of the control group was male (n=12) and 60% was female (n=18). The mean age of the control group was 50.6±17.3 years, with a minimum age of

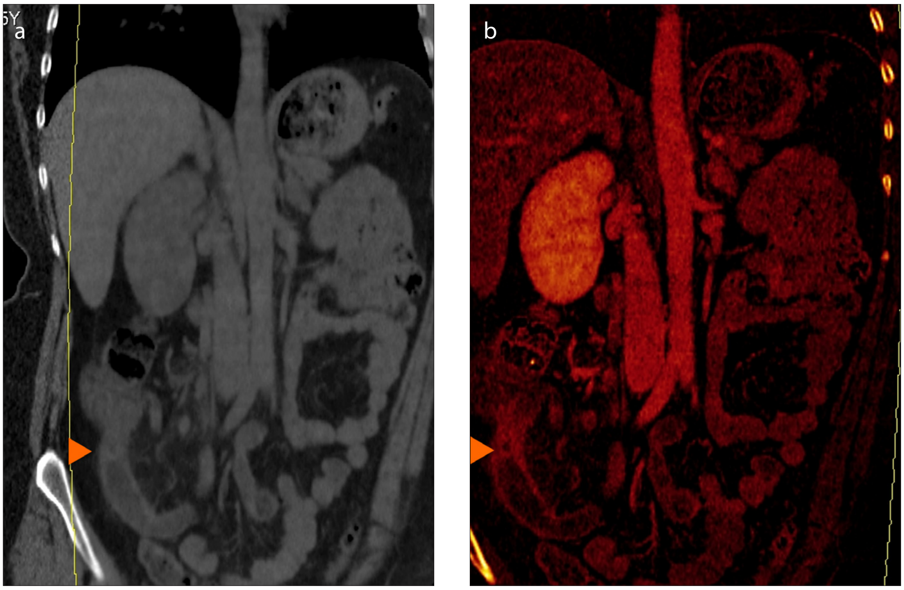

Figure 3. a, b. In dual-energy computed tomography (DECT), virtual noncontrast (VNC) images are easily reconstructed without extra scans. VNC image **(a)** reveals a distended appendix *(arrowhead)*. Iodine map image **(b)** demonstrates increased iodine uptake *(arrowhead)* in the appendiceal wall due to inflammation. Note the slight hyperattenuation of the inflamed appendiceal wall in the VNC image.

Table 1. Patient characteristics of both groups

Parameters	Group	Male, n (%)	Female, n (%)
Gender	Control, n=30	12 (40)	18 (60)
	Appendicitis, n=26	12 (46)	14 (54)
		Mean±SD	Range
Age (years)	Control	50.6±17.3	23–85
	Appendicitis	36.3±14.1	18–66
Maximum appendiceal diameter (mm)	Control	5.7±0.5	4.6–6.8
	Appendicitis	11.5±2.3	7.5–16.8

SD, standard deviation.

23 years and a maximum age of 85 years. Patient characteristics of both groups are summarized in Table 1.

The mean appendiceal diameter in the patient group was 11.5±2.3 mm (range, 7.5–16.8 mm). In the control group, the mean appendiceal diameter was 5.7±0.5 mm (range, 4.6–6.8 mm). The difference between the mean appendiceal diameters of the two groups was statistically significant ($P < 0.001$) (Table 1).

In the patient group, the mean density measured in the VNC images was 20.7±11.7 HU (range, -10.1 to 46.3 HU) (Fig. 3). In the control group, the mean density was 1.4±16.6 HU (range, -50.9 to 16.9 HU). The mean density of the inflamed appendices was significantly higher than healthy appendices ($P < 0.001$) (Table 2). The overall diagnostic performance of VNC images was found to be good in the ROC analysis (AUC 0.834; $P < 0.001$). For the threshold value of > 7.5 HU, sensitivity, specificity, PPV, and NPV rates were 93.3%, 66.6%, 73.7%, 90.9%, respectively (Table 3).

In the patient group, the median density measured in the overlay images was 48.9 HU (range, 34.1–78.3 HU; IQR, 13.7 HU) (Fig. 3). In the control group, the median density was 37.3 HU (range, 10.0–9.8; IQR, 10.0 HU). The median density of inflamed appendices was significantly higher than the median density of normal appendices ($P < 0.001$) (Table 2). The overall diagnostic performance of overlay images was found to be good in the ROC analysis (AUC 0.847; $P < 0.001$). For the threshold value of >44.2 HU, the sensitivity, specificity, PPV, and NPV rates were 73.3%, 90%, 88%, 77.1%, respectively (Table 3).

In the patient group, the mean density measured in the 80 kVp images was 101.5±20.1 HU (range, 67.5–146.3 HU) (Fig. 4). In the control group, the mean density was 52.6±12.3 HU (range, 23.1–73.3 HU). The mean density of inflamed appendices was significantly higher than the mean density of healthy appendices ($P < 0.001$) (Table 2). The overall diagnostic performance of 80 kVp images was found to be excellent in the ROC analysis (AUC 0.996; $P < 0.001$). Among all image sets, 80 kVp images demonstrated the highest diagnostic performance. For the threshold value of >69 HU, the sensitivity, specificity, PPV, and NPV rates were 96.6%, 96.6%, 96.7%, 96.7%, respectively (Table 3).

In the patient group, the mean density measured in the 140 kVp images was 59.5±13.7 HU (range, 28.2–86.6 HU) (Fig. 4). In the control group, the mean density was 31.1±13.4 HU (range, 7.4–66.8 HU). The mean density of inflamed appendices was significantly higher than the mean density of healthy appendices ($P < 0.001$) (Table 2). The overall diagnostic performance of 140 kVp images was found to be excellent in the ROC analysis (AUC 0.929; $P < 0.001$). For the threshold value of >42.1 HU, the sensitivity, specificity, PPV, and NPV rates were 96.6%, 86.6%, 87.9%, 96.3%, respectively (Table 3).

The mixed (standard) image set was the default image set used to evaluate the appendix vermiformis. In the patient group, the mean density measured in the mixed images was 71.9±15.9 HU (range, 36.5–107.9 HU) (Fig. 4). In the control group, the mean density was 38.3±11.7 HU (range, 17.8–66.8 HU). The mean density of inflamed appendices was significantly higher than the mean density of healthy appendices ($P < 0.001$) (Table 2). The overall diagnostic performance of mixed images was found to be excellent in the ROC analysis (AUC 0.951; $P < 0.001$) For the threshold value of >52.8 HU, the sensitivity, specificity, PPV, and NPV rates were 93.3%, 90%, 90.3%, 93.1%, respectively (Table 3).

Among virtual monoenergetic images, the 70 keV images demonstrated the highest diagnostic accuracy (AUC 0.958; $P < 0.001$). In the patient group, the mean density measured in the 70 keV images was 79.1±15.5 HU (range, 47.3–117.9 HU). In the control group, the mean density was 46.7±10.8 HU (range, 29.2–70.9 HU). The mean density of inflamed appendices was significantly higher than the mean density of healthy appendices (*P* < 0.001) (Table 2). For the threshold value of >63.6 HU, the sensitivity, specificity, PPV, and NPV rates were 90%, 90%, 90%, 90%, respectively (Table 3).

The median/mean densities of virtual monoenergetic images obtained at 40 keV, 50 keV, 60 keV, 70 keV, 80 keV, 90 keV, and 100 keV images (Fig. 5) are presented in Table 2. The median/mean densities of the inflamed appendices were significantly higher than the median/mean densities of the healthy appendices in all VMI image sets (*P* < 0.001) (Table 2). The overall diagnostic performance was found to be good at 40 keV (AUC 0.880; *P* < 0.001), 50 keV (AUC 0.898; *P* < 0.001) and 60 keV (AUC 0.897; *P* < 0.001), and excellent at 70 keV (AUC 0.958; *P* < 0.001), 80 keV (AUC 0.934; *P* < 0.001), 90 keV (AUC 0.907; *P* < 0.001) and 100 keV (AUC 0.904; *P* < 0.001) in the ROC analysis. AUC values are presented in Table 3 and Fig. 6.

Inter-rater agreement for the two researchers was good at 80 kVp images (ICC, 0.78; 95%CI, 0.73–0.84; *P* < 0.001).

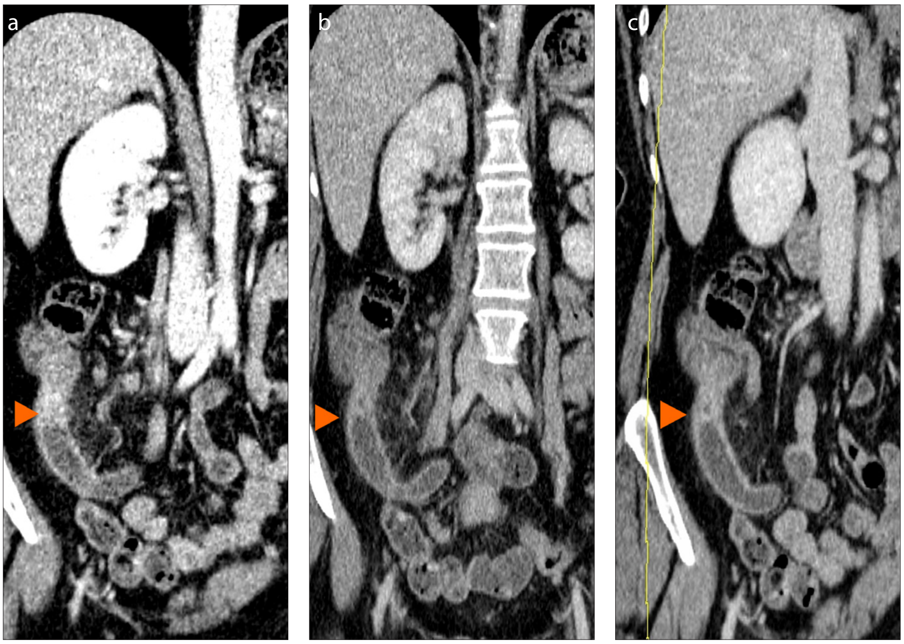

Figure 4. a–c. Acute appendicitis *(arrowhead)* in the 80 kVp **(a)**, 140 kVp **(b)**, and fusion/mixed **(c)** images. The contrast enhancement *(arrowhead)* due to inflammation is more obvious in the 80 kVp images **(a)** than the 140 kVp **(b)** and fusion/mixed **(c)** images.

Discussion

The present study was designed to evaluate the diagnostic value of DECT imaging in patients with AA. Abdominal DECT examinations were performed at voltages of 80 kVp and 140 kVp. The mean densities measured on 80 kVp images in the patient group were significantly higher than those measured on 140 kVp images, as the K edge of iodine (33.2 keV) is closer to 80 kVp than it is to 140 kVp. The diagnostic performance of DECT at 80 kVp was higher than at 140 kVp, thus enabling more confident detection of increased appendiceal wall enhancement (Fig. 4).

It has been reported that VNC images of inflammatory pathologies of the intestinal wall do not contribute to diagnosis (17). On the other hand, in our study, the mean densities of the inflamed appendices were significantly higher than those of healthy appendices in the VNC images. It is postulated that hyperattenuation of the intestinal wall affected by intestinal ischemia might occur due to hyperperfusion or intramural hemorrhage (18). The relatively high densities detected in VNC images of the inflamed appendix, may be due to the same underlying pathophysiology. Hyperemia in the

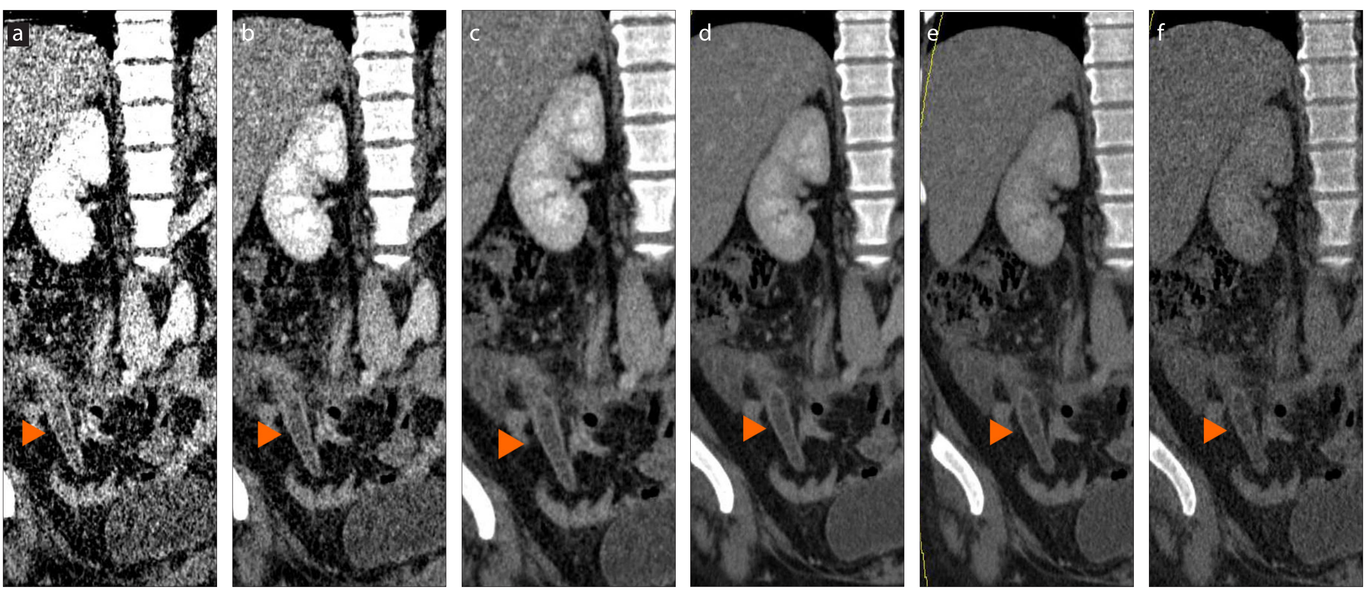

Figure 5. a–f. Virtual monochromatic images can be reconstructed at different energy levels using the wide-range X-ray energy levels in DECT. Obvious higher noise rates at lower energy levels are apparent, with higher contrast enhancement *(arrowheads)*. Appendiceal inflammation is best appreciated at energy levels of 60–80 keV: **(a)** 40 keV; **(b)** 50 keV; **(c)** 60 keV; **(d)** 70 keV; **(e)** 80 keV; **(f)** 90 keV images.

Table 2. Comparison of appendiceal densities in the control and appendicitis groups at different energy levels and image sets

Image sets	Group	Mean±SD or Median (IQR) HU	Range HU
80 kVp	Normal	52.6±12.3	23.1–73.3
	Appendicitis	101.5±20.1	67.5–146.3
140 kVp	Normal	31.1±13.4	7.4–66.8
	Appendicitis	59.5±13.7	28.2–86.6
VNC	Normal	1.4±16.6	-50.9 to 16.9
	Appendicitis	20.7±11.7	-10.1 to 46.3
Overlay*	Normal	37.3 (10)	9.8–85.8
	Appendicitis	48.9 (13.7)	34.1–78.3
Mixed	Normal	38.3±11.7	17.9–64.6
	Appendicitis	71.9±15.9	36.5–107.9
40 keV*	Normal	146 (39.5)	64.7–348
	Appendicitis	196.3 (50.4)	139–306.2
50 keV*	Normal	97.9 (22.6)	51.1–218
	Appendicitis	136.1 (28.5)	51.2–218
60 keV	Normal	69.4±20.4	34.2–129
	Appendicitis	103.4±19.2	68.5–151.3
70 keV	Normal	46.7±10.8	29.2–70.9
	Appendicitis	79.1±15.5	47.3–117.9
80 keV	Normal	38.6±10.2	23.8–61
	Appendicitis	64.6±31.6	31.6–92.5
90 keV	Normal	31.8 ±12	10–54.2
	Appendicitis	55.1 ±12.6	22.4–86.3
100 keV	Normal	26.3±12.5	2.5–51.4
	Appendicitis	48.9±12.9	17.3–88.6

All *P* values are <0.001 for the comparison of normal and appendicitis groups.
SD, standard deviation; IQR, interquartile range; HU, Hounsfiled Unit; kVp, kilovoltage peak; VNC, virtual noncontrast image; keV, kiloelectron volt.
*Median values with interquartile range due to non-normal distribution.

appendiceal wall, intramural hemorrhage, or densitometric contamination by intraluminal fecaloid content may be considered factors contributing to this increased HU value (Fig. 3).

DECT enables quantitative assessment of "iodine content" in the intestinal wall, which can improve the diagnostic success of imaging in diagnosing diseases affecting the intestinal wall by detecting differences in enhancement. We could not measure the iodine content in the appendiceal wall due to the absence of dedicated software; consequently, we were not able to assess the utility of iodine content measurement in the diagnosis of AA. On the other hand, in the overlay (iodine map) and mixed images, the densities of the inflamed appendices were significantly higher than those of the healthy appendices. Overlay and mixed images were found to have good and excellent diagnostic performances, respectively. However, the diagnostic accuracies of these two sets of images lagged behind the 80 kVp images, in which AUC value was the highest.

Images generated at different keV energy levels can be used to maximize contrast between tissues or to better visualize iodine in tissue. In our study, healthy and inflamed appendiceal densities in the range of 40 keV and 100 keV energy levels with increments of 10 keV were measured. Inflamed appendiceal densities were significantly higher than healthy appendiceal densities at all intervals. Although we did not study signal-to-noise (SNR) or contrast-to-noise (CNR) values, it is reported that image noise increases progressively as the energy level deviates from the 60–70 keV spectrum (energy levels <60 keV or >70 keV). However, at higher keV energy levels, beam hardening artifacts decrease, whereas at low keV energy levels, maximization of contrast is observed due to the K-value of iodine at approximately 33 keV (19). Despite monitoring iodine contrast maximization at low energy levels, low image quality due to increased noise appears to emerge as a problem due to existing reconstruction algorithms (20) (Fig. 5).

When we analyzed the 40 keV and 50 keV images, the highest densities were measured due to the increased photoelectric interaction of iodine at low energy levels. The diagnostic performance of these energy levels, in which the density of the inflamed appendix is highest, is calculated to be lower than the higher energy levels, but still with satisfactory diagnostic performance. Despite increased iodine attenuation, the reduced SNR in these images is believed to be an underlying reason for reduced diagnostic value (19). In our study, we found that the energy level with the highest diagnostic performance among the monoenergetic image sets was 70 keV. The diagnostic value reached the highest level at 70 keV, then gradually decreased. This finding can support a previous study in which CNR was reported to be highest at 70 keV and SNR was reported to be highest at 80 keV (21). Other studies have reported that the optimal energy level for soft tissue evaluation ranges from 60 to 77 keV (19).

Ultrasonography remains the primary diagnostic tool for appendicitis, with a safer profile for patients; however, CT is used in cases for which sonograms are negative or inconclusive. At this point, it is important to perform CT with the lowest possible radiation exposure and yet with acceptable diagnostic quality. The sensitivity, specificity,

Table 3. The threshold values of DECT image sets in the diagnosis of AA

Image sets	Threshold	Youden Index-J	Sensitivity 95% CI	Specificity 95% CI	PPV	NPV	AUC* 95% CI
80 kVp	>69	0.93	96.6 82.8–99.9	96.6 82.8–99.9	96.7 80.8–99.5	96.7 80.8–99.5	0.996 0.986–1.000
140 kVp	>42.1	0.83	96.6 82.8–99.9	86.6 69.3–96.2	87.9 74.4–94.8	96.3 79.0–99.4	0.929 0.859–0.999
VNC	>7.5	0.60	93.3 77.9–99.2	66.6 47.2–82.7	73.7 62.6–82.4	90.9 71.9–97.5	0.834 0.729–0.938
Overlay (iodine)	>44.2	0.63	73.3 54.1–87.7	90.0 73.5–97.9	88.0 71.0–95.6	77.1 64.8–86.1	0.847 0.744–0.950
Mixed	>52.8	0.83	93.3 77.9–99.2	90.0 73.5–97.9	90.3 76.1–96.5	93.1 77.9–98.1	0.951 0.900–0.1000
40 keV	>169.8	0.73	86.6 69.3–96.2	86.6 69.3–96.2	86.67 69.3–96.2	86.67 69.3–96.2	0.880 0.787–0.973
50 keV	>127	0.70	80.0 61.4–92.3	90.0 73.5–97.9	88.9 72.9–96.0	81.8 68.5–90.3	0.898 0.813–0.983
60 keV	>85.4	0.73	83.3 65.3–94.4	90.0 73.5–97.9	89.3 73.8–96.1	84.4 70.6–92.4	0.897 0.811–0.983
70 keV	>63.6	0.80	90.0 73.5–97.9	90.0 73.5–97.9	90.00 73.5–97.9	90.00 73.5–97.9	0.958 0.914–1.000
80 keV	>51.3	0.76	86.6 69.3–96.2	90.0 73.5–97.9	89.7 74.6–96.2	87.1 72.9–94.4	0.934 0.873–0.996
90 keV	>40.7	0.70	93.3 77.9–99.2	76.6 57.7–90.1	80.0 67.5–88.5	92.0 74.8–97.8	0.907 0.831–0.982
100 keV	>37.9	0.73	90.0 73.5–97.9	83.3 65.3–94.4	84.4 70.6–92.4	89.3 73.8–96.1	0.904 0.826–0.982

The threshold value corresponding with the Youden index J is the optimal threshold value as disease prevalence is 50% in the study; thus equal weight is given to sensitivity and specificity, and the costs of various decisions are ignored.
DECT, dual-energy computed tomography; AA, acute appendicitis; CI, confidence interval; PPV, positive predictive value; NPV, negative predictive value; AUC, area under the ROC curve; kVp, kilovoltage peak; keV, kiloelectron volt; VNC, virtual noncontrast image.
* $P < 0.001$.

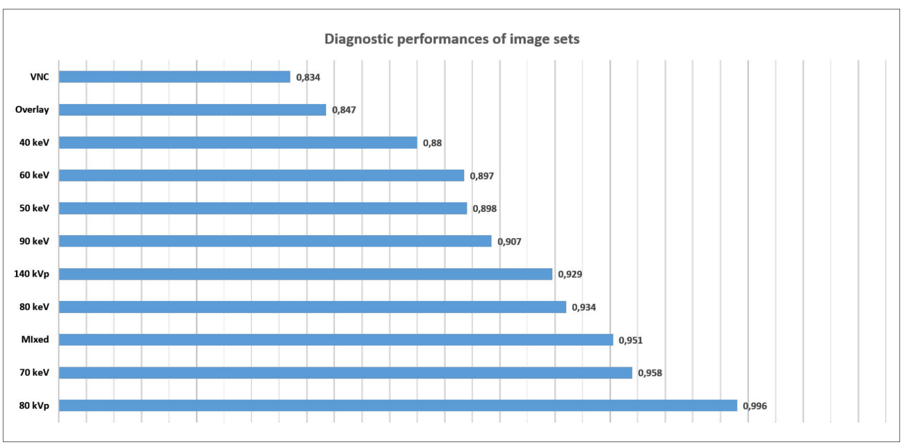

Figure 6. Bar chart of the area under the receiver operating characteristic curve (AUC) values of image sets. The 80 kVp image set yielded the best diagnostic performance, while 70 keV images demonstrated the highest diagnostic performance among the virtual monoenergetic image sets.

PPV, NPV, and diagnostic performance rates imply that the 80 kVp image set of DECT is more useful in the diagnosis of AA compared with the mixed CT image set which can be regarded as conventional CT scans (Table 3, Fig. 6). This result may be helpful in reducing radiation dose because any decrease in tube potential provides more of a decrease in the overall radiation dose compared with any reduction in tube current. The performance of monoenergetic 70 keV and 80 keV image sets were also better than the 140 kV image data set, which implies that low keV CT scanning may be preferred for the diagnosis of AA. This approach appears to provide higher diagnostic performance in addition to reduction in the overall radiation burden to patients.

There were limitations to our study. The number of individuals in the patient and control groups was relatively small and insufficient to obtain definitive cutoff density values for the image sets. It is critically important that the first measurements are performed by two readers in consensus at the same time. Although the inter-rater agreement was found to be good at 80 kVp images, measurements would be assessed in terms of consistency and reproducibility among different observers at different times. Therefore, the lack of several independent readings of the CT examinations and measurements of appendiceal wall density may have decreased the validity of this study. Because the ROI measurements were performed at the most compressed site of the appendix rather than at the appendiceal wall itself, luminal density may have affected the final measurement within or among cases. Using automatic tube current modulation would prevent standardization of density measurements through the samples. However, automatic tube modulation is a standard technical feature of modern CT scanners given that they are being more frequently used in abdominal imaging to reduce patient radiation exposure. Using constant mAs in all patients would also prevent standardization of density measurements since the variability of patient thickness causes a wide range of density measurements in the absence of tube modulation. The effect of patient body mass index or abdominal circumference on SNR or CNR were not evaluated. Evaluation of SNR on different keV images would enable better interpretation of image quality. Because the onset of patient symptoms and the time to CT scan were not recorded, the effect of this potential factor on appendiceal density could not be investigated. Although we attempted to standardize the amount of contrast agent used for CT scans according to patient weight, the effect of the patient's body mass index on the density measurement could not be examined. Rather than a direct measurement of appendiceal densities, a proportional densitometry measurement could provide more accurate results by determining an anatomical reference point with less variable density (such as the aorta).

In conclusion, evaluation of DECT imaging suggested that low tube voltage with 80 kVp had high diagnostic performance, which indicates low kVp CT scanning may be useful for the diagnosis of AA with reduced patient exposure to radiation.

Conflict of interest disclosure

The authors declared no conflicts of interest.

References

1. Flum DR, Koepsell T. The clinical and economic correlates of misdiagnosed appendicitis: Nationwide analysis. Arch Surg 2002; 137:799–804. [CrossRef]
2. Terasawa T, Blackmore CC, Bent S, Kohlwes RJ. Systematic review: computed tomography and ultrasonography to detect acute appendicitis in adults and adolescents. Ann Intern Med 2004; 141:537–546. [CrossRef]
3. Malone AJ, Jr., Wolf CR, Malmed AS, Melliere BF. Diagnosis of acute appendicitis: value of unenhanced CT. AJR Am J Roentgenol 1993; 160:763–766. [CrossRef]
4. Lane MJ, Katz DS, Ross BA, Clautice-Engle TL, Mindelzun RE, Jeffrey RB, Jr. Unenhanced helical CT for suspected acute appendicitis. AJR Am J Roentgenol 1997; 168:405–409. [CrossRef]
5. Rao PM, Rhea JT, Novelline RA, Mostafavi AA, Lawrason JN, McCabe CJ. Helical CT combined with contrast material administered only through the colon for imaging of suspected appendicitis. AJR Am J Roentgenol 1997; 169:1275–1280. [CrossRef]
6. Choi D, Park H, Lee YR, et al. The most useful findings for diagnosing acute appendicitis on contrast-enhanced helical CT. Acta Radiol 2003; 44:574–582. [CrossRef]
7. Fletcher JG, Takahashi N, Hartman R, et al. Dual-energy and dual-source CT: is there a role in the abdomen and pelvis? Radiol Clin North Am 2009; 47:41–57. [CrossRef]
8. Karçaaltincaba M, Aktas A. Dual-energy CT revisited with multidetector CT: review of principles and clinical applications. Diagn Interv Radiol 2011; 17:181. [CrossRef]
9. Yu L, Leng S, McCollough CH. Dual-energy CT-based monochromatic imaging. AJR Am J Roentgenol 2012; 199(Suppl 5):S9–S15. [CrossRef]
10. Balthazar EJ, Birnbaum BA, Yee J, Megibow AJ, Roshkow J, Gray C. Acute appendicitis: CT and US correlation in 100 patients. Radiology 1994; 190:31–35. [CrossRef]
11. Balthazar E, Megibow A, Siegel S, Birnbaum B. Appendicitis: prospective evaluation with high-resolution CT. Radiology 1991; 180:21–24. [CrossRef]
12. Weltman DI, Yu J, Krumenacker J, Jr, Huang S, Moh P. Diagnosis of Acute Appendicitis: Comparison of 5- and 10-mm CT Sections in the Same Patient. Radiology 2000; 216:172–177. [CrossRef]
13. Rao PM, Rhea JT, Novelline RA, Mostafavi AA, Lawrason JN, McCabe CJ. Helical CT combined with contrast material administered only through the colon for imaging of suspected appendicitis. AJR Am J Roentgenol 1997; 169:1275–1280. [CrossRef]
14. Birnbaum BA, Balthazar EJ. CT of appendicitis and diverticulitis. Radiol Clin North Am 1994; 32:885.
15. Birnbaum BA, Jeffrey Jr RB. CT and sonographic evaluation of acute right lower quadrant abdominal pain. AJR Am J Roentgenol 1998; 170:361–371. [CrossRef]
16. Carr NJ. The pathology of acute appendicitis. Ann Diagn Pathol 2000; 4:46-58. [CrossRef]
17. Fulwadhva UP, Wortman JR, Sodickson AD. Use of dual-energy CT and iodine maps in evaluation of bowel disease. Radiographics 2016; 36:393–406. [CrossRef]
18. Wiesner W, Khurana B, Ji H, Ros PR. CT of acute bowel ischemia. Radiology 2003; 226:635–650. [CrossRef]
19. Yu L, Christner JA, Leng S, Wang J, Fletcher JG, McCollough CH. Virtual monochromatic imaging in dual-source dual-energy CT: radiation dose and image quality. Med Phys 2011; 38:6371–6379. [CrossRef]
20. Matsumoto K, Jinzaki M, Tanami Y, Ueno A, Yamada M, Kuribayashi S. Virtual monochromatic spectral imaging with fast kilovoltage switching: improved image quality as compared with that obtained with conventional 120-kVp CT. Radiology 2011; 259:257–262. [CrossRef]
21. Darras KE, McLaughlin PD, Kang H, et al. Virtual monoenergetic reconstruction of contrast-enhanced dual energy CT at 70keV maximizes mural enhancement in acute small bowel obstruction. Eur J Radiol 2016; 85:950–956. [CrossRef]